PSO-Based Self-Commissioning of Electrical Motor Drives

Marco Calvini, Mauro Carpita, *Member, IEEE*, Andrea Formentini, and Mario Marchesoni, *Member, IEEE*

***Abstract*—A new method for electrical motor drive self-commissioning, with elastic couplings and backlash, is presented. The heuristic algorithm particle swarm optimization (PSO) has been used for the identification and optimization of parameters. Initially, a model-based identification procedure is performed to evaluate the parameters of the system. Then, the parameters of a proportional–integral–derivative (PID)-based controller are optimized by using a time-domain performance criterion. Experimental results, obtained by testing three different laboratory permanent magnet synchronous motor (PMSM) drive prototypes, are also presented to confirm the validity of the proposed approach.**

***Index Terms*—Backlash, particle swarm optimization (PSO), permanent-magnet synchronous motor (PMSM) drive, self-commissioning.**

I. Introduction

ELECTRICAL motors, particularly permanent-magnet synchronous motors (PMSMs), are widely used in automation and robotic applications. Their high power density and reliability make this type of motor very common in industrial applications such as numerical controlled machines, paper and plastic machines, industrial manipulators, etc. In recent years, a lot of attention has been spent to improve the dynamic response of industrial machines to increase productivity. However, the presence of transmission elements, such as gears or elastic shafts, could highly affect the performance of the drive system. A simple solution is to remove or limit the use of this kind of elements, but often, it is not structurally possible. Therefore, it is necessary to develop controllers that are able to take into account these types of mechanical imperfections and to compensate them. Until now, the commissioning of an industrial plant is almost always accomplished by qualified personnel using manual time-consuming procedures.

A self-commissioning system should be able to optimize the drive controller to obtain the best dynamic response from the system. To this aim, it should perform two main tasks: the system modeling and identification and the optimal controller synthesis.

With reference to the first task, frequency-domain methods have been proposed in the literature [1], [2]. However, these methods cannot be used in the presence of system nonlinearities like backlash and friction. In this regard, a comparison of the identification method is presented in [3]. The use of a genetic algorithm is proposed in [4] for a drive-load system identification and the optimal controller synthesis. A simple strategy to identify only the gap size of the backlash is proposed in [5].

In [6] and [7], comparative studies of different control strategies developed in order to face the problem of torsional oscillation have been presented. A predictive control approach to control a PMSM has been presented in [8] and [9], while the use of state estimators has been adopted in [10] and [11]. Within this scenario, proportional–integral–derivative (PID) controllers are still widespread in industries, in part due to the still limited computational capabilities of some industrial drives and also because of their effectiveness. For this reason, different works have been presented in recent years to optimize the PID-based controller parameters [12]–[16].

However, in almost all of these works, the presence of the backlash nonlinearities has not been taken into account. Some solutions to compensate the presence of backlash have been proposed in [17]–[22].

A complete self-commissioning procedure for electrical motor drives, with particular reference to PMSM drives, capable of both identifying the system and synthesizing the optimal controller parameters, is here presented. As shown in some other works [23]–[25], heuristic algorithms have demonstrated good results to accomplish identification and optimization tasks. In this paper, the particle swarm optimization (PSO) has been chosen due to its simple implementation and its low computational cost, which are important characteristics considering the industrial needs. PSO is a heuristic search method that has recently found application in different fields including power electronics [26]–[33].

In Section II, an overview of the PSO algorithm is presented. In Section III, the model used during both the identification and optimization steps is described. The identification task is a gray-box model-based approach and is described in Section IV. Due to its still wide diffusion in industrial systems, a PID-based controller has been adopted. In Section V, its structure is presented along with the parameter optimization procedure. All results have been validated using experimental prototypes and are presented in Section VI.

Manuscript received April 8, 2013; revised July 23, 2013, November 14, 2013, March 27, 2014, and May 16, 2014; accepted May 24, 2014. Date of publication August 20, 2014; date of current version January 7, 2015.

M. Calvini is with Phase Motion Control S.p.A., 16141 Genoa, Italy (e-mail: marco.calvini@phase.eu).

M. Carpita is with the University of Applied Sciences of Western Switzerland, 1400 Yverdon-les-Bains, Switzerland (e-mail: mauro.carpita@heig-vd.ch).

A. Formentini and M. Marchesoni are with the Department of Electrical, Electronic, Telecommunications Engineering and Naval Architecture, University of Genoa, 16145 Genoa, Italy (e-mail: andrea.formentini@unige.it; marchesoni@unige.it).

Color versions of one or more of the figures in this paper are available online at http://ieeexplore.ieee.org.

Digital Object Identifier 10.1109/TIE.2014.2349478

II. PSO

PSO is a relatively new heuristic search method which utilizes a set of agents (particles) to find the global minimum of an objective function. In the last years, it has attracted the interest of many researchers due to its simple implementation and efficiency to solve high-dimensional problems and handle functions with many local minimum points.

PSO is based on a swarm of particles which, at the beginning of the algorithm, are randomly distributed on the state space. At each iteration, every particle updates its speed, depending on the local optimum found by the particle and the global optimum found by the swarm. Usually, the algorithm stops when a fixed number of iterations has been reached. Since its first proposal in 1995 [34], different variants of the algorithm have been proposed [35]. After some empirical tests, the version described in [26] has been used in this work, and it is summarized by the following steps.

1) The speed and position of each particle are initialized to random values between speed and position bounds, respectively.
2) For each particle, the cost function is evaluated in its current position.
3) The values computed at the previous point are compared with the particle best cost c_l. If the current cost value is better than c_l, it becomes the new particle best cost, and the particle best position $\underline{x}_l \in \mathbb{R}^n$ is updated with the current particle position.
4) The particle with the best c_l is identified: Its cost becomes the swarm best cost c_g, and its position becomes the swarm best position $\underline{x}_g \in \mathbb{R}^n$.
5) Every particle's speed is updated using the following equation:

$$\underline{v}_{k+1} = w\underline{v}_k + \phi_1 R_1(\underline{x}_l - \underline{x}_k) + \phi_2 R_2(\underline{x}_g - \underline{x}_k) \quad (1)$$

where $\underline{v}_k \in \mathbb{R}^n$ and $\underline{x}_k \in \mathbb{R}^n$ are respectively the speed and position of the particle at the kth iteration, ϕ_1 and ϕ_2 are the acceleration constants, $\underline{x}_l \in \mathbb{R}^n$ and $\underline{x}_g \in \mathbb{R}^n$ are respectively the current local optimal position and the current global optimal position, $R_1 \in \mathbb{R}^{nxn}$ and $R_2 \in \mathbb{R}^{nxn}$ are two diagonal matrices where each element r_i is a random number $\in [0, 1]$, and w is the inertia constant.

6) Each particle's position is updated

$$\underline{x}_{k+1} = \underline{x}_k + \underline{v}_{k+1}. \quad (2)$$

Both speed and position are bounded. The value $\underline{v}_b = 0.1(\underline{x}_{\max} - \underline{x}_{\min})$ is used as the bound of the speed absolute value.

7) The steps from 2) to 6) are repeated until $k \leq k_{\max}$, where $k_{\max}$ is the maximum number of iterations.

Different solutions have been proposed about the choice of the algorithm parameters [36]. In this paper, a dynamic inertia constant

$$w_k = w_{\max} - \frac{w_{\max} - w_{\min}}{k_{\max}} k \quad (3)$$

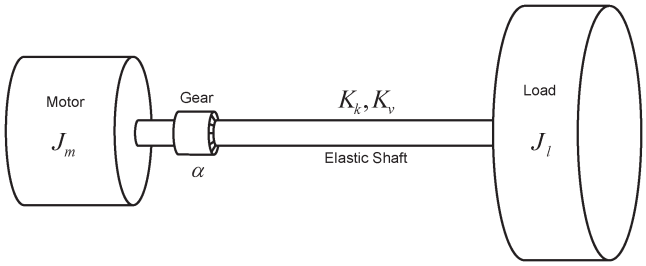

Fig. 1. Schematic representation of a two-mass system with backlash.

with $w_{\max} = 0.9$ and $w_{\min} = 0.4$ has been utilized. The two acceleration constants have been set to $\phi_1 = \phi_2 = 2$.

III. System Model

The system model is used in the identification and optimization process. It is therefore very important to choose the right model to obtain good performance. Different models have been proposed in the technical literature to describe systems with elastic elements and gears. After many tests, the dynamic model described by the following equations has been chosen:

$$\begin{cases} \dot{\omega}_m = \frac{1}{J_m}\left(I_q K_t - T - B_m\omega_m - D_m sign(w_m)\right) \\ \dot{\theta} = w_m \\ \dot{\omega}_l = \frac{1}{J_l}\left(T - T_l - B_l w_l - D_l sign(w_l)\right) \\ \dot{\theta} = \omega_l \end{cases} \quad (4)$$

where θ_m and θ_l are respectively the motor and load angular positions, ω_m and ω_l are the motor and load angular speeds, I_q is the motor quadrature current, K_t is the motor torque constant, T_l is the load-side torque disturbance, J_m and J_l are the motor and the load inertia, B_m and D_m are the motor-side viscous and Coulomb frictions, and B_l and D_l are the load-side viscous and Coulomb frictions. Moreover, the shaft torque T is described by the model proposed by Nordin in [37]

$$T = K_k(\theta_d - \theta_b) + K_v(\dot{\theta}_d - \dot{\theta}_b) \quad (5)$$

where

$$\theta_d = (\theta_m - \theta_l). \quad (6)$$

θ_b is an auxiliary variable whose dynamics is governed by the following equation:

$$\dot{\theta}_b = \begin{cases} \max\left(0, \dot{\theta}_b + \left(\frac{K_k}{K_v}\right)(\theta_d - \theta_b)\right), & \theta_b = -\alpha \\ \dot{\theta}_b + \left(\frac{K_k}{K_v}\right)(\theta_d - \theta_b), & |\theta_b| < \alpha \\ \min\left(0, \dot{\theta}_b + \left(\frac{K_k}{K_v}\right)(\theta_d - \theta_b)\right), & \theta_b = \alpha \end{cases} \quad (7)$$

where K_k and K_v are the stiffness and internal damping of the shaft, while 2α is the gap between the gear teeth.

The model describes a two-mass system where the two masses are connected to each other between a gear and an elastic element, as schematized in Fig. 1.

IV. System Identification

The first step of the commissioning is the identification of the system that is to be controlled. A test signal $u(t)$, corresponding to the quadrature current reference, is applied to the plant to be identified, while the output response $y(t) = \omega_m(t)$ is recorded. The same input signal is then used as input to the system models described in the next sections. The model output is $y_r(t, \underline{p}_i)$, where $\underline{p}_i$ is the vector of free parameters to be identified. A cost function $J(\underline{p}_i)$ has been defined as

$$J(\underline{p}_i) = \sum_{i=0}^{N} \left(y(t_i) - y_r(t_i, \underline{p}_i) \right)^2 \tag{8}$$

where t_i represents the ith sampling instant and N refers to the number of samples of $u(t)$ and $y(t)$. The PSO algorithm is used to discover the optimal set of parameters $\underline{p}_i^{opt}$ that minimizes $J(\underline{p}_i)$.

To obtain a better estimation of the parameters, the identification procedure is split into two steps.

A. Low-Frequency Identification

In the first phase, the plant and the model are fed by a low-pass-filtered pseudo random binary signal (PRBS) with a low number of torque sign inversions, with a bandwidth equal to 10 Hz. This permits to reduce the excitation of both the elastic elements and the backlash of the gears and allows to obtain a good identification of the total inertia and of the total frictions of the system. During this phase, a reduced model of the system is used. It is governed by the following equation:

$$\dot{\omega} = \frac{1}{J_{tot}} \left(I_q K_t - T_l - B_{tot}\omega - D_{tot} sign(\omega) \right). \tag{9}$$

The corresponding parameter vector is

$$\underline{p}_i^1 = [J_{tot} \quad B_{tot} \quad D_{tot}]. \tag{10}$$

B. High-Frequency Identification

The identification of the high-frequency parameters has been divided in two subcategories, depending on the backlash presence.

1) Absence of Backlash: If no gear is present in the plant or if the backlash is small enough to be neglected, a PRBS is used as excitation signal. In this case, the parameter α is set to zero, and consequently, $\theta_b(t) = 0 \; \forall t$. A constant component is added to the PRBS to keep rotating the system and avoiding that static Coulomb friction affects the identification.

To minimize the number of free parameters, the inertia ratio is defined as

$$R_J = \frac{J_m}{J_l} \tag{11}$$

and consequently

$$J_m = \frac{R_J}{R_J + 1} J_{tot} \qquad J_l = \frac{1}{R_J + 1} J_{tot}. \tag{12}$$

Since frictions are usually nondominant elements, it is a good approximation to define

$$B_m = B_l = \frac{B_{tot}}{2} \qquad D_m = D_l = \frac{D_{tot}}{2}. \tag{13}$$

In this phase, the parameter vector is defined as

$$\underline{p}_i^2 = [R_J \quad K_k \quad K_v]. \tag{14}$$

The definition of the inertia ratio permits to use the already identified parameter J_{tot} and, consequently, to reduce the number of free parameters.

2) Backlash Identification: In the presence of backlash, the system becomes highly nonlinear, and the use of a PRBS is no longer effective. When the backlash gap is open, there is no information about load position. Therefore, to permit a good identification, the system is kept fed by a constant torque. This guarantees that the gap is closed, and therefore, the relative position between the load and the motor is known. A torque pulse, with a different sign from the constant component, has been used as excitation signal. This type of procedure guarantees the opening of the backlash gap starting from a known position. In this case, the parameter vector is set to

$$\underline{p}_i^3 = [R_J \quad K_k \quad K_v \quad \alpha]. \tag{15}$$

V. Controller Structure and Tuning

Fig. 2 shows the block scheme of the whole drive control system. The controller is PID based, with proportional and derivative gains split in feedforward gains (K_{Vff}, K_{Aff}) and feedback gains (K_{Vfb}, K_{Afb}), while K_P is the integral gain. This solution allows it to have two degrees of freedom more than a classical PID, with almost the same computational complexity. Additionally, the integrative contribution has been computed using the read shaft position as shown in Fig. 2. This configuration permits to avoid the use of the cascade of the derivative and the integral of the read position that may lead to a shaft rotational drift at zero speed due to numerical error. In this paper, only the motor-side position is considered available since the rotor position is also needed to implement the field-oriented control. A more performing state feedback control could be implemented using an additional load-side sensor, but this solution would reduce the reliability of the system and would increase the costs. The goal of this work is to obtain the best possible performance using a simple controller such as the PID. The low-pass filter (LPF) block represents a second-order Butterworth low-pass filter, with cutoff frequency f_{LP}, used to attenuate both high frequency resonances and measurement noise. The block Mec corresponds to the mechanical dynamics of the system as described by (4)–(7). The block El represents the inner proportional–integral (PI) current loop dynamic response. Since the electrical dynamic response is usually faster than the mechanical one, it is a good approximation to assume that the current regulation loop is not affected by the mechanical configuration of the plant. For this reason, the identification of the electrical parameters and the consequent tuning of the controller can be done in a precommissioning phase that will

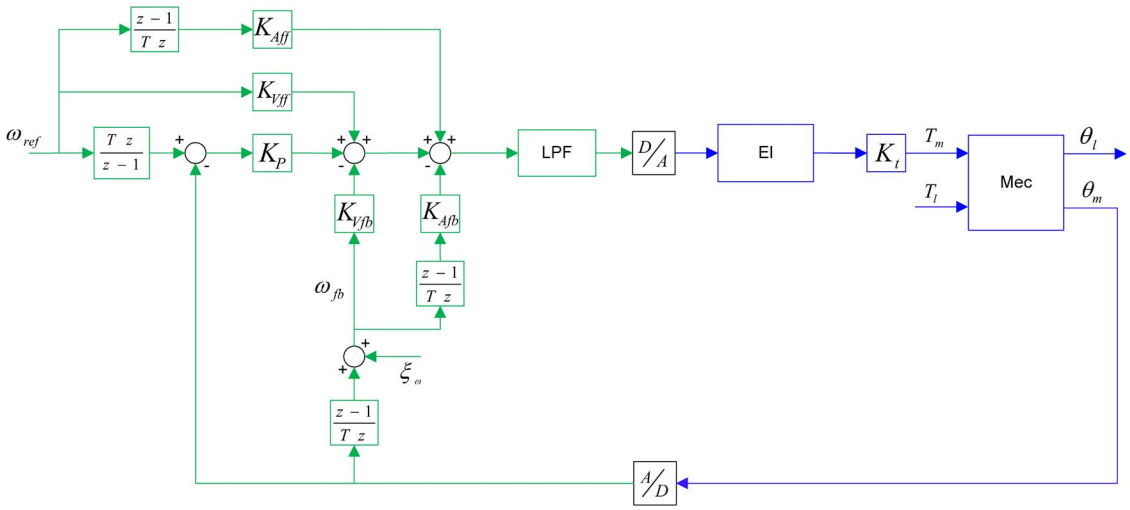

Fig. 2. Digital control block diagram—blue paths and blocks represent the continuous system, while green ones correspond to the digital controller.

not be described in detail. A procedure similar to the one used for the mechanical part has been adopted in this work to find the parameter model and to tune the current loop. The latter has been approximated as a second-order system of equation

$$El(z) = \frac{0.2664z + 0.6611}{z^2 - 0.1415 + 0.9948}. \tag{16}$$

Finally, ξ_ω is the measurement noise.

To tune the controller parameters, an iterative procedure based on the PSO algorithm has been used in a similar way to the identification one. The system shown in Fig. 2 has been simulated, and the system responses, obtained by varying the controller parameters, have been analyzed. A weighted cost function has been defined as

$$J(\underline{p}_c, \underline{c}) = st + c_1 \cdot stl + c_2 \cdot d\omega + c_3 \cdot os \tag{17}$$

where $\underline{p}_c$ is the free parameter vector defined as

$$\underline{p}_c = [K_{Vff} \quad K_{Vfb} \quad K_p \quad K_{Aff} \quad K_{Afb} \quad f_{LP}] \tag{18}$$

$$\underline{c} = [c_1 \quad c_2 \quad c_3] \tag{19}$$

is the weight parameter vector. The free parameters (18) to be optimized do not explicitly appear in cost function (17). Such parameters, however, influence the system response and, consequently, the single term that compose the cost function.

The optimization procedure is carried out simulating the system model previously identified. Two different simulation tests are needed to compute the cost (17).

The first one simulates the system response subject to a reference step variation from $\omega_{ref}(t) = -A_r$ to $\omega_{ref}(t) = A_r$, where A_r is a generic constant that depends on the system characteristics. A change in speed direction implies at least a change in the sign of torque and, therefore, a change in the excitation of the backlash. A guideline for choosing these values and obtaining a good optimization is to impose a reference step variation that does not cause a current saturation. In fact, the regulator is no longer able to properly control the system dynamics when its output is saturated, and therefore, the optimization procedure could produce a nonoptimal set of parameters. Similarly, during the operation of the plant, a prefilter should be added to the reference signal to avoid control saturation and obtain the optimal performance from the regulator.

The two terms st and os in (17) are respectively the settling time and the overshoot of the load speed. The third term in (17) is defined as

$$d\omega = \sum_i |\omega_m(t_i) - \omega_l(t_i)|\,. \tag{20}$$

It forces the system to reduce the difference between the load speed and motor speed and, consequently, to damp oscillations. The reduction of speed difference also decreases the shaft torsion and, therefore, the mechanical stress of the system. The second test simulates the response of the system rotating at a constant speed Ω and subject to a load step disturbance $T_l(t) = A_l$, with A_l being the generic constant. The stl term in (17) is the settling time of the load speed to the reference value Ω after the disturbance occurs. It keeps in consideration the time that the system takes to go back to the reference speed after a torque load is applied to the shaft. It is, in general, different from the st time that the system takes to reach the reference speed after a reference step variation.

The use of these time-domain performance indicators simplifies the setting of the weight parameters. Indeed, an indicative value for the terms $c_i (i = 1, 2, 3)$ is the reciprocal of the expected value of the corresponding performance indicator. The tool will try to set the controller parameters in order to satisfy the desired performance. In case it is not possible, it will make a compromise based on how far the single performance indicators are from the expected values. Varying the weights in (17), it is possible to balance the importance of the single performance parameter and, consequently, the dynamic response of the system.

The weight vectors used in the experiments described hereinafter are reported in Table I.

The optimal controller parameter vector $\underline{p}_c^{opt}$ is found by minimizing the cost function (17).

TABLE I
COST FUNCTION WEIGHT PARAMETERS

	c_1	c_2	c_3
1st Set-up	1	0	0.5
2nd Set-up	1	3.5	0.5
3rd Set-up	2.5	0	0.5

TABLE II
MOTOR PARAMETERS

Parameter	Value	Units
Nominal Torque	40	Nm
Max speed	300	$\text{rad} \cdot \text{s}^{-1}$
Rotor Inertia	$2.4 \cdot 10^{-3}$	kgm^2
K_t	1.2	$\text{Nm} \cdot \text{A}_{\text{rms}}^{-1}$

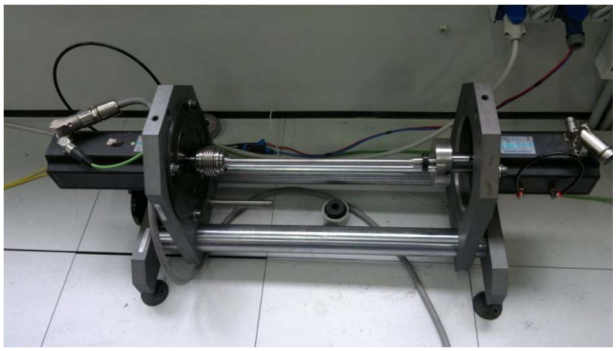

Fig. 3. First experimental setup.

VI. EXPERIMENTAL RESULTS

Three different experimental prototypes have been built and used to validate the proposed commissioning tool.

They are composed by two equal PMSM drives connected together by different mechanical couplings. The main motor parameters are shown in Table II. The control has been implemented on a fixed point digital signal processor, and the sampling time has been chosen to be equal to $T = 1.25 \cdot 10^{-4}$ s. The motor position θ_m has been measured using a 32-b/rev optical encoder because it is already mounted on the experimental setup. However, is worth noting that such a high precision is not needed.

During both the identification and optimization PSO tasks, a population of 30 particles and a limit of 1000 iterations have been used. Increasing the particles and/or the iteration number increases the probability to find the optimal solution but, at the same time, also increases the computation time of the algorithm. The aforementioned two parameters have been empirically found as a good compromise between computation time and quality of solutions. The tool is thought to run offline, and it will be integrated with the human-machine-interface software. For this reason, it has been tested on a Pentium 4 Dual-Core 1.8 GHz. Both the identification and optimization tasks lasted about 60 s each.

The first experimental setup is shown in Fig. 3. It is composed by the two motors connected by a long elastic shaft. The load inertia has been increased by using a flywheel. The coupling has been achieved with an elastic joint so that no backlash is present.

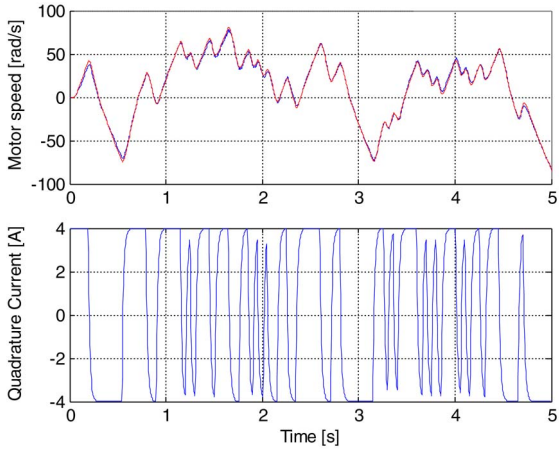

Fig. 4. Up: Comparison between the (blue) first experimental setup and (red) its one-mass model responses. Down: Excitation signal constituted by a low-frequency PRBS, with quadrature current i_q proportional to motor torque.

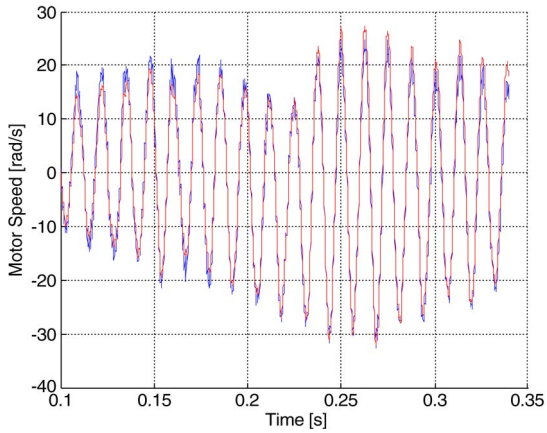

Fig. 5. Comparison between the (blue) first experimental setup and (red) its model responses applying as input a quadrature current i_q constituted by a high-frequency PRBS.

TABLE III
FIRST SETUP IDENTIFIED PARAMETERS

Parameter	Value	Units
J_{tot}	0.01162	kgm^2
K_k	541.6	$\text{Nm} \cdot \text{rad}^{-1}$
K_v	0.008512	$\text{Nms} \cdot \text{rad}^{-1}$
B_{tot}	0.01182	$\text{Nms} \cdot \text{rad}^{-1}$
D_{tot}	0.7958	Nm
R_J	0.3488	-

The identification procedure has been carried out as described in Section IV. Initially, the system has been modeled as a one-mass system. In Fig. 4, a comparison of the real system with the identified reduced model is shown, where a good matching can be appreciated. In such a figure, the excitation signal, constituted by a low-frequency PRBS, is also shown.

Subsequently, the full-order system described by (4)–(7) has been considered. Considering the absence of the backlash, the parameter α has been set to 0, and a high-frequency PRBS excitation signal has been used as plotted in Fig. 5. The identified system parameters are reported in Table III.

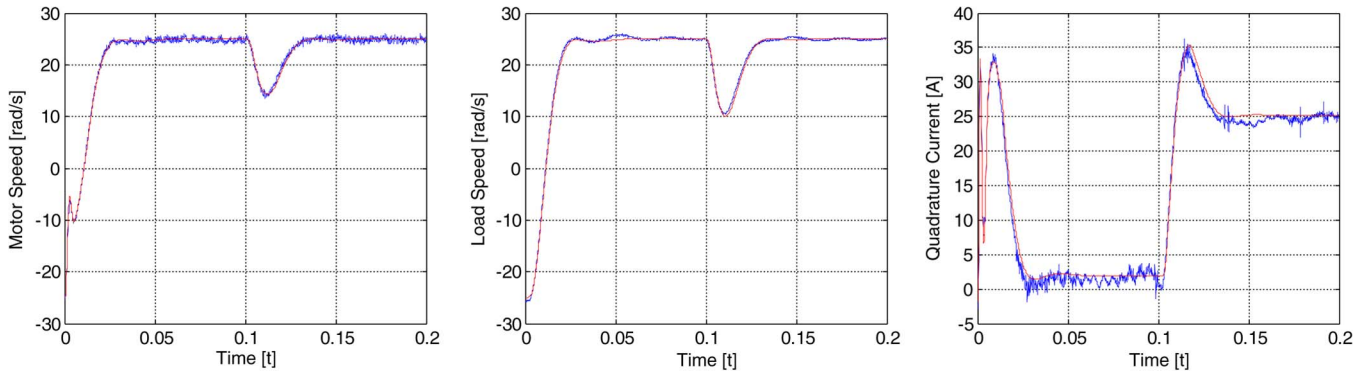

Fig. 6. Comparison between (blue) first experimental setup and (red) its model responses after the controller parameter optimization.

TABLE IV
FIRST SETUP CONTROLLER OPTIMAL PARAMETERS

Parameter	Value	Units
K_{Vff}	0.68	$\mathrm{As \cdot rad^{-1}}$
K_{Vfb}	2.15	$\mathrm{As \cdot rad^{-1}}$
K_{Aff}	0	$\mathrm{As^2 \cdot rad^{-1}}$
K_{Afb}	0	$\mathrm{As^2 \cdot rad^{-1}}$
K_p	149	$\mathrm{A \cdot rad^{-1}}$
f_{LP}	500	Hz

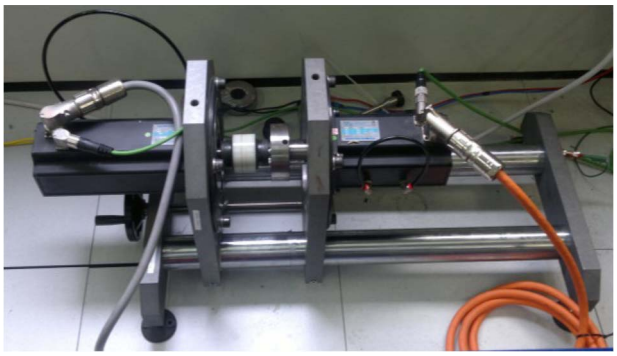

Fig. 7. Second experimental setup.

The controller optimization procedure described in Section V has been then applied. The low-pass filter upper bound cutoff frequency has been fixed to 500 Hz to eliminate high frequency resonances and noise. The results of the optimization process are plotted in Fig. 6 and reported in Table IV. A speed reference variation has been imposed from -25 to 25 rad/s. The latter value has been chosen, according to Section V, to avoid the current saturation. The optimal controller, after being synthesized, has been tested on the whole drive speed range with good results.

A load torque disturbance of 30 N · m (75% of the nominal torque) has been applied at a time equal to 0.1 s. Fig. 6 allows to notice a very good response. Both responses to speed reference variation and to torque loading last about 30 ms, and no overshoot is present. A very good matching between the model and the real system responses can also be noted.

A second experimental setup has been then developed. The same main motor and load motor have been connected through a gear, as shown in Fig. 7. The identification results related to the low-frequency parameters have been omitted in this case

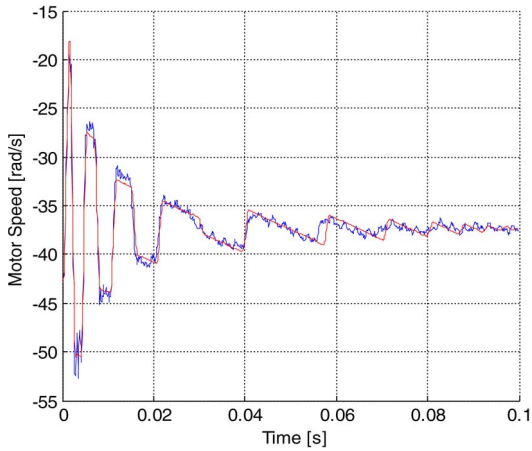

Fig. 8. Open-loop impulse response of (blue) the second experimental setup and (red) its model one after the identification process.

TABLE V
SECOND SETUP IDENTIFIED PARAMETERS

Parameter	Value	Units
J_{tot}	0.01186	$\mathrm{kgm^2}$
K_k	11259	$\mathrm{Nm \cdot rad^{-1}}$
K_v	1.33	$\mathrm{Nms \cdot rad^{-1}}$
B_{tot}	0.01012	$\mathrm{Nms \cdot rad^{-1}}$
D_{tot}	0.81	Nm
R_J	0.2817	-
α	0.5692	deg

because they are very similar to the previous ones. However, the presence of the gear introduces a backlash in the system that must be taken into account during the identification of the high-frequency parameters. Fig. 8 shows the system response to a 50-A quadrature current impulse, generating a torque opposite to the rotation speed, as explained in Section IV-B. The identified parameters are reported in Table V. After the identification process, the controller parameters have been optimized using the model with backlash. A speed reference step variation from -10 to 10 rad/s has been chosen in order to avoid the current saturation. In fact, when the speed controller output saturates, the controller is no longer able to effectively control the system behavior. As it can be deduced from Fig. 9, very good dynamic responses and matching between the model and real system have been obtained. A strongly nonlinear behavior can also

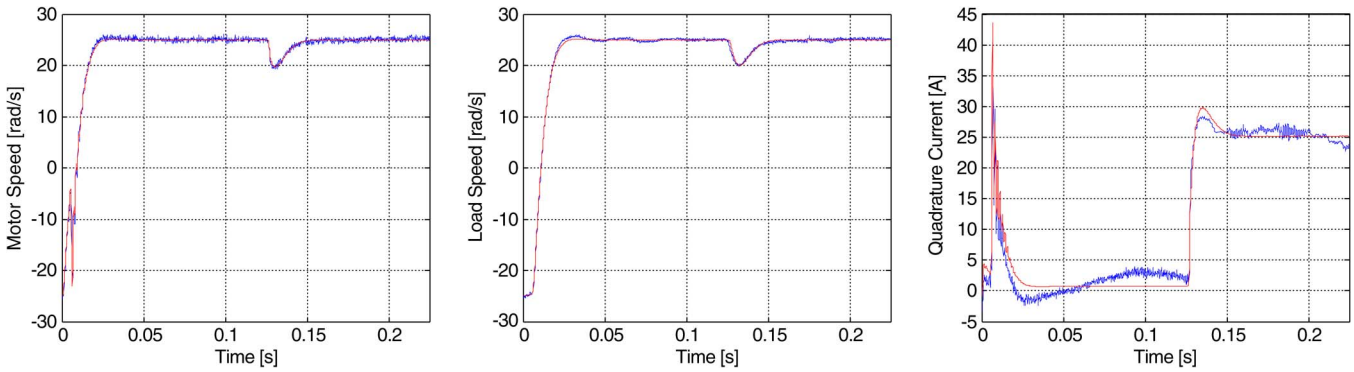

Fig. 9. Comparison between (blue) second experimental setup and (red) its model responses after the controller parameter optimization.

TABLE VI
SECOND SETUP CONTROLLER OPTIMAL PARAMETERS

Parameter	Value	Units
K_{Vff}	0	$\mathrm{As}\cdot\mathrm{rad}^{-1}$
K_{Vfb}	3.83	$\mathrm{As}\cdot\mathrm{rad}^{-1}$
K_{Aff}	0	$\mathrm{As}^2\cdot\mathrm{rad}^{-1}$
K_{Afb}	0.001024	$\mathrm{As}^2\cdot\mathrm{rad}^{-1}$
K_p	413	$\mathrm{A}\cdot\mathrm{rad}^{-1}$
f_{LP}	500	Hz

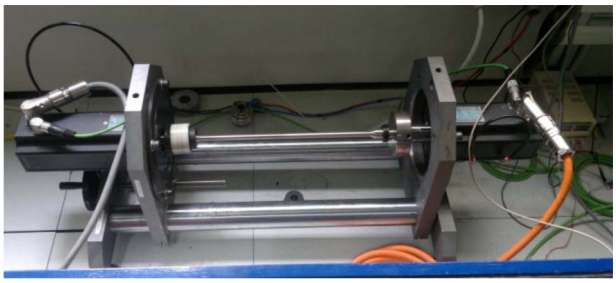

Fig. 10. Third experimental setup.

TABLE VII
THIRD SETUP IDENTIFIED PARAMETERS

Parameter	Value	Units
J_{tot}	0.01167	kgm^2
K_k	614	$\mathrm{Nm}\cdot\mathrm{rad}^{-1}$
K_v	1.33	$\mathrm{Nms}\cdot\mathrm{rad}^{-1}$
B_{tot}	0.00637	$\mathrm{Nms}\cdot\mathrm{rad}^{-1}$
D_{tot}	0.9755	Nm
R_J	0.3493	-
α	0.7481	deg

TABLE VIII
SETUP PARAMETER COMPARISON

	First Set-up	Second Set-up	Third Set-up	Units
K_k	541.6	11259	614	$\mathrm{Nm}\cdot\mathrm{rad}^{-1}$
K_v	0.008512	1.33	1.33	$\mathrm{Nms}\cdot\mathrm{rad}^{-1}$
R_J	0.3488	0.2817	0.3493	-
α	none	0.5692	0.7481	deg

TABLE IX
THIRD SETUP CONTROLLER OPTIMAL PARAMETERS

Parameter	Value	Units
K_{Vff}	0.2054	$As\cdot rad^{-1}$
K_{Vfb}	2.62	$As\cdot rad^{-1}$
K_{Aff}	0	$As^2\cdot rad^{-1}$
K_{Afb}	0.002571	$As^2\cdot rad^{-1}$
K_p	184.2	$A\cdot rad^{-1}$
f_{LP}	500	Hz

be noted in the motor speed plot due to the presence of the backlash. As soon as the speed reference changes, the motor accelerates strongly in the opposite rotation direction. During this phase, it is no longer connected to the load due to the presence of the backlash. This is confirmed by the fact that the load speed is still almost constant and equal to -10 rad/s. At about 0.005 s, the motor gets connected with the load again, it decelerates, and an oscillatory trend is generated due to the presence of the elastic shaft. At this point, the load speed starts to change, too. The more smooth trend of the load speed is due to the low inertia ratio that filters the discontinuous variation of the motor speed. The optimal controller parameters obtained are reported in Table VI.

In this configuration, the absence of a long shaft gives a high stiffness to the system. Subsequently, it has been considered interesting to analyze the proposed procedure in the presence of both backlash and mechanical transmission low stiffness. In the third experimental setup, the long shaft has been then reintegrated while maintaining the gear, as shown in Fig. 10. The system parameters have been identified as described earlier and are reported in Table VII. Additionally, a comparison among the three setups' high-frequency parameters is reported in Table VIII. The identification results have been omitted because they are very similar to the ones related to the second experimental setup. The optimization of the controller has been executed, and the optimal values of the controller parameters that have been obtained are displayed in Table IX. Fig. 11 shows that, also in this case, a good transient response, except a slight overshoot in the real load speed after the reference change, and a satisfactory matching between the model and the plant have been obtained.

VII. CONCLUSION

In this paper, a complete self-commissioning procedure for both the identification and control optimization of a PMSM drive has been proposed. The presence of nonstiff transmission

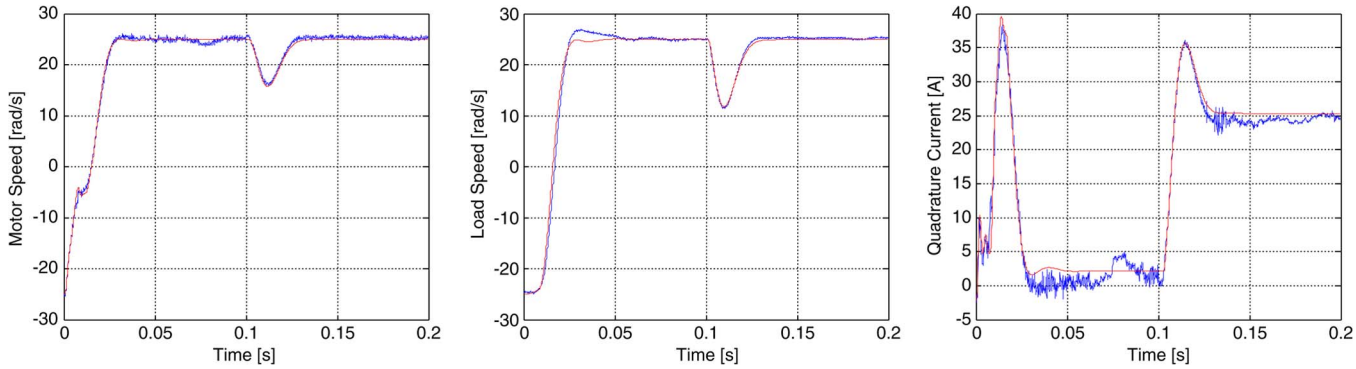

Fig. 11. Comparison between (blue) third experimental setup and (red) its model responses after the controller parameter optimization.

elements, which may cause mechanical resonances, has been taken into account. The nonlinearities introduced by gearboxes have been considered as well. All results have been validated by using three experimental prototypes, and they show the effectiveness of the proposed method.

REFERENCES

[1] M. Zigliotto and L. Peretti, "Identification of mechanical load for electrical drives commissioning—Labeling machine case study," in *Proc. IEEE EUROCON*, St. Petersburg, Russia, 2009, pp. 797–803.

[2] R. Krishnan, T. Bjazic, and P. Crnosija, "Optimization of PM brushless dc motor drive speed controller using modification of Ziegler-Nichols methods based on bode plots," in *Proc. 12th EPE-PEMC*, 2006, pp. 343–348.

[3] E. Schutte, H. Wertz, H. Grotstolben, and S. Beineke, "Comparison of parameter identification schemes for self-commissioning drive control of nonlinear two-mass systems," in *Conf. Rec. IEEE IAS Annu. Meeting*, Oct. 1997, vol. 1, pp. 493–500.

[4] P. Zanchetta, M. Sumner, and N. Okaeme, "Robust control design through experimental load identification for variable speed drives," in *Conf. Rec. IEEE IAS Annu. Meeting*, Sep. 2007, pp. 1257–1264.

[5] M. Pacas and S. Villwock, "Time-domain identification method for detecting mechanical backlash in electrical drives," *IEEE Trans. Ind. Electron.*, vol. 56, no. 2, pp. 568–573, Feb. 2009.

[6] T. Orlowska-Kowalska and K. Szabat, "Vibration suppression in a two-mass drive system using PI speed controller and additional feedbacks—Comparative study," *IEEE Trans. Ind. Electron.*, vol. 54, no. 2, pp. 1193–1206, Apr. 2007.

[7] N. Hoffmann, F. W. Fuchs, and S. Thomsen, "PI control, PI-based state space control, and model-based predictive control for drive systems with elastically coupled loads—A comparative study," *IEEE Trans. Ind. Electron.*, vol. 58, no. 8, pp. 3647–3657, Aug. 2011.

[8] K. Szabat and P. J. Serkies, "Application of the MPC controller to the position control of the two-mass drive system," *IEEE Trans. Ind. Electron.*, vol. 60, no. 9, pp. 3679–3688, Sep. 2013.

[9] C. A. Silva, J. I. Yuz, and E. J. Fuentes, "Predictive speed control of a two-mass system driven by a permanent magnet synchronous motor," *IEEE Trans. Ind. Electron.*, vol. 59, no. 7, pp. 2840–2848, Jul. 2012.

[10] T. Orlowska-Kowalska and K. Szabat, "Application of the Kalman filters to the high-performance drive system with elastic coupling," *IEEE Trans. Ind. Electron.*, vol. 59, no. 11, pp. 4226–4235, Nov. 2012.

[11] I. Scholing, B. Orlik, and K. Peter, "Robust output-feedback H∞ control with a nonlinear observer for a two-mass system," *IEEE Trans. Ind. Appl.*, vol. 39, no. 3, pp. 637–644, May/Jun. 2003.

[12] D. Candusso, D. Hissel, J. M. Kauffmann, and M. C. Pera, "Enhanced servo-control performance of dual-mass systems," *IEEE Trans. Ind. Electron.*, vol. 54, no. 3, pp. 1387–1399, Jun. 2007.

[13] J. Deskur and R. Muszynski, "Damping of torsional vibrations in high-dynamic industrial drives," *IEEE Trans. Ind. Electron.*, vol. 57, no. 2, pp. 544–552, Feb. 2010.

[14] J. Cao, Y. Qiao, and C. Ma, "Polynomial method based design of low-order controllers for two-mass system," *IEEE Trans. Ind. Electron.*, vol. 60, no. 3, pp. 969–978, Mar. 2013.

[15] G. Zhang, "Speed control of two-inertia system by PI/PID control," *IEEE Trans. Ind. Electron.*, vol. 47, no. 3, pp. 603–609, Jun. 2000.

[16] X. Jiao, J. Zhang, and T. Shen, "An adaptive servo control strategy for automotive electronic throttle and experimental validation," *IEEE Trans. Ind. Electron.*, vol. 61, no. 11, pp. 6275–6284, Nov. 2014.

[17] P. O. Gutman and M. Nordin, "Nonlinear speed control of elastic systems with backlash," in *Proc. 39th IEEE Conf. Decision Control*, Dec. 2000, vol. 4, pp. 4060–4065.

[18] Y. Hori and M. Chengbin, "Backlash vibration suppression in torsional system based on the fractional order Q-filter of disturbance observer," in *Proc. 8th IEEE AMC*, Mar. 2004, pp. 577–582.

[19] E. Mohammadiasl, "Vibration detection and backlash suppression in machine tools," in *Proc. IEEE/RSJ IROS*, Oct. 2009, pp. 972–977.

[20] M. Itoh, "Torsional vibration suppression of a twin-drive geared system using model-based control," in *Proc. 10th IEEE AMC*, Mar. 2008, pp. 176–181.

[21] F. M. Malik, K. Munawar, and M. B. Khan, "Switched hybrid speed control of elastic systems with backlash," in *Proc. IEEE IEEM*, Dec. 2010, pp. 1641–1644.

[22] A. N. Safacas, E. D. Mitronikas, and I. X. Bogiatzidis, "Detection of backlash phenomena appearing in a single cement kiln drive using the current and the electromagnetic torque signature," *IEEE Trans. Ind. Electron.*, vol. 60, no. 8, pp. 3441–3453, Aug. 2013.

[23] M. Iwasaki, N. Matsui, and K. Itoh, "Optimal design of robust vibration suppression controller using genetic algorithms," *IEEE Trans. Ind. Electron.*, vol. 51, no. 5, pp. 947–953, Oct. 2004.

[24] G. L. Cascella, F. Neri, N. Salvatore, M. Sumner, and A. Caponio, "A fast adaptive memetic algorithm for online and offline control design of PMSM drives," *IEEE Trans. Syst., Man, Cybern. B, Cybern.*, vol. 37, no. 1, pp. 28–41, Feb. 2007.

[25] A. Formentini, G. Maragliano, M. Marchesoni, and M. Calvini, "Self-commissioning of direct drive systems," in *Proc. SPEEDAM*, Jun. 2012, pp. 1348–1353.

[26] G. K. Venayagamoorthy, S. Mohagheghi, J. C. Hernandez, and Y. Del Valle, "Particle swarm optimization: Basic concepts, variants and applications in power systems," *IEEE Trans. Evol. Comput.*, vol. 12, no. 2, pp. 191–175, Apr. 2008.

[27] Z.-L. Gaing, "A particle swarm optimization approach for optimum design of PID controller in AVR system," *IEEE Trans. Energy Convers.*, vol. 19, no. 2, pp. 384–391, Jun. 2004.

[28] Z. Salam and K. Ishaque, "A deterministic particle swarm optimization maximum power point tracker for photovoltaic system under partial shading condition," *IEEE Trans. Ind. Electron.*, vol. 60, no. 8, pp. 3195–3206, Aug. 2013.

[29] C. H. Liu and Y. Y. Hsu, "Design of a self-tuning PI controller for a STATCOM using particle swarm optimization," *IEEE Trans. Ind. Electron.*, vol. 57, no. 2, pp. 702–715, Feb. 2010.

[30] W. Chen, Y. Wang, S. Liu, J. Jia, and Q. Li, "Parameter identification for PEM fuel-cell mechanism model based on effective informed adaptive particle swarm optimization," *IEEE Trans. Ind. Electron.*, vol. 58, no. 6, pp. 2410–2419, Jun. 2011.

[31] H. T. Yau, Y. C. Tian, and C. J. Lin, "Identification and compensation of nonlinear friction characteristics and precision control for a linear motor stage," *IEEE/ASME Trans. Mechatronics*, vol. 18, no. 4, pp. 1385–1396, Aug. 2013.

[32] S. Bhaumik, S. N. Singh, and D. Saxena, "Identification of multiple harmonic sources in power system using optimally placed voltage measurement devices," *IEEE Trans. Ind. Electron.*, vol. 61, no. 5, pp. 2483–2492, May 2014.

[33] K. Shen *et al.*, "Elimination of harmonics in a modular multilevel converter using particle swarm optimization-based staircase modulation strategy," *IEEE Trans. Ind. Electron.*, vol. 61, no. 10, pp. 5311–5322, Oct. 2014.
[34] R. Eberhart and J. Kennedy, "Particle swarm optimization," in *Proc. IEEE Int. Conf. Neural Netw.*, 1995, vol. 4, pp. 1942–1948.
[35] K. Kameyama, "Particle swarm optimization—A survey," *IEICE Trans. Inf. Syst.*, vol. E92.D, no. 7, pp. 1354–1361, Jul. 2009.
[36] M. El-Hawary, A. Sallam, A. Kalas, and A. El-Gallad, "Enhancing the particle swarm optimizer via proper parameters selection," in *Proc. Can. Conf. Electron. Comput. Eng.*, 2002, pp. 792–797.
[37] J. Galic, P. Gutman, and M. Nordin, "New models for backlash and gear play," *Int. J. Adaptive Control Signal Process.*, vol. 11, no. 1, pp. 49–63, 1997.

Marco Calvini received the M.S. degree in electrical engineering from the University of Genoa, Genoa, Italy, in 1988 for his work in power electronics applied to motion control.

After an initial experience in teaching, he joined Phase Motion Control S.p.A., Genoa, as Head of R&D and Chief Scientist. In his position, he contributed to the development of the company's advanced servo drives, from the initial ASIC integrated circuit drives, to the development of the first generation of fully digital drives (AXV series) which set a standard for high dynamics. Later work performed under his coordination span from high-efficiency high-power photovoltaic converters to dedicated drives for hybrid traction and high-performance underwater vessels. He is the holder of numerous patents in the field of power conversion and currently alternates his activity between the China and Italy R&D teams of the company.

Mauro Carpita (M'99) received the M.S. and Ph.D. degrees in electrical engineering from the University of Genoa, Genoa, Italy, in 1985 and 1989, respectively.

Following graduation, he was working with the corporate research unit of Ansaldo (Genoa) in the field of converters for drives and power quality. From 1997 to 1999, he was with Lincoln Electric (Savona) as a Technical Office Manager of power electronics welding machines. From 1999 to 2003, he was with ABB Ricerca (Milan) and, later, with ABB Servomotors (Asti) as a Senior Scientist working in the field of servo and very-high-speed drives. Since 2003, he has been a Professor with the University of Applied Sciences, Yverdon-les-Bains, Switzerland. His research interests are mainly devoted to high-voltage converters and power electronics for drives and smart grid applications. He is the holder of four industrial patents.

Dr. Carpita is a member of the European Power Electronics (EPE) Association.

Andrea Formentini was born in Genoa, Italy, in 1985. He received the M.S. degree in computer engineering and the Ph.D. degree in electrical engineering from the University of Genoa, Genoa, in 2010 and 2014, respectively.

He is currently working as a Research Fellow in the Power Electronics, Transportation and Automation Laboratory, University of Genoa. His research interests include control systems applied to electrical machine drives and power converters.

Mario Marchesoni (M'89) received the M.S. degree (with honors) in electrical engineering and the Ph.D. degree in electrical engineering in power electronics from the University of Genoa, Genoa, Italy, in 1986 and 1990, respectively.

Following graduation, he began his research activity with the Department of Electrical Engineering, University of Genoa, where he was an Assistant Professor from 1992 to 1995. From 1995 to 2000, he was with the Department of Electric and Electronic Engineering, University of Cagliari, Cagliari, Italy, where he was a Full Professor of power industrial electronics. Since 2000, he has been with the University of Genoa, where he is currently a Full Professor of electrical drives control. He is the author or coauthor of more than 160 papers. His research interests include power electronics, rotating machinery, and automatic control, particularly in high-power converters and electrical drives.

Prof. Marchesoni is a member of the EPE Executive Council.